Asymmetric micro-Doppler frequency comb generation via magnetoelectric coupling

Dmitry Filonov,[1,2] Ben Z. Steinberg,[1] and Pavel Ginzburg[1,2,*]

[1]*School of Electrical Engineering, Tel Aviv University, Tel Aviv 69978, Israel*

[2]*Information Technologies, Mechanics and Optics (ITMO) University, St. Petersburg 197101, Russia*

(Received 19 December 2016; revised manuscript received 23 February 2017; published 22 June 2017)

Electromagnetic scattering from moving bodies, being an inherently time-dependent phenomenon, gives rise to a generation of new frequencies, which can be used to characterize the motion. Whereas an ordinary motion along a linear path produces a constant Doppler shift, an accelerated scatterer can generate a micro-Doppler frequency comb. The spectra produced by rotating objects were studied and observed in a bistatic lock-in detection scheme. The internal geometry of a scatterer was shown to determine the spectrum, and the degree of structural asymmetry was suggested to be identified via signatures in the micro-Doppler comb. In particular, hybrid magnetoelectric particles, showing an ultimate degree of asymmetry in forward and backward scattering directions, were investigated. It was shown that the comb in the backward direction has signatures at the fundamental rotation frequency and its odd harmonics, whereas the comb of the forward scattered field has a prevailing peak at the doubled frequency and its multiples. Additional features of the comb were shown to be affected by the dimensions of the particle and by the strength of the magnetoelectric coupling. Experimental verification was performed with a printed circuit board antenna based on a wire and a split ring, while the structure was illuminated at a 2 GHz carrier frequency. Detailed analysis of micro-Doppler combs enables remote detection of asymmetric features of distant objects and could find use in a span of applications, including stellar radiometry and radio identification.

DOI: 10.1103/PhysRevB.95.235139

I. INTRODUCTION

Investigation of electromagnetic processes in moving coordinate systems requires applying a certain set of transformations to the laws of electrodynamics formulated for reference frames at rest [1]. Relativistic effects could substantially change the regular form of Maxwell's equations, material constitutive relations, and boundary conditions, especially in the case of accelerated motion, which in the most general case, requires applying the formalism of the general theory of relativity [2]. Nevertheless, the majority of practical applications take place in regimes of slow motion and acceleration, where simplifying approximations can be applied. One of the practical examples dealing with nonrelativistic scenarios is radio detection and ranging (radar), where distant objects are probed with short pulses. Time delay between transmitted and received pulses enables extracting the range, while Doppler shifts hold information about velocities [3]. Approximate electromagnetic analysis of the phenomenon relies on a set of static simulations, stitched together along a mechanical path of an object. Here, this approach will be referred to as *adiabatic*. Full characterization of a mechanical motion also requires knowledge of accelerations, which can be estimated using additional spectral analysis. For example, techniques for detection of helicopter propellers (axial rotation implies accelerated motion) exist [4–6]. Accelerated bodies, in contrast to uniformly moving objects, produce much richer spectral signatures, called micro-Doppler shifts [7]. Recently, micro-Doppler combs generated by axially rotating wires and split ring resonators (SRRs) were investigated [8,9]. In particular, objects illuminated by a field of frequency ω generate a frequency comb at a scattered field: the peaks are equidistant and situated at $\omega \pm n\Omega$, where Ω is the angular frequency of rotation and n is an integer number. It is worth noting that the additional spectral features are generated by time-varying boundary conditions. Furthermore, it was shown that phase retardation effects along a rotating scatterer control the amplitudes of the peaks in the comb. Along with the phase accumulation effects, the symmetry properties of an object have crucial importance. For example, scatterers possessing reflection symmetry and rotating around their centers cannot generate even peaks in the comb. The degree of asymmetry is important for remote characterization of distant moving objects, and its impact will be investigated here by the example of an asymmetric scatterer.

The frequency combs produced by asymmetric rotating objects are studied theoretically, numerically, and observed experimentally with a lock-in detection scheme. The main emphasis here is on electromagnetically small objects. It is shown that the micro-Doppler combs generated by asymmetric scatterers strongly depend on the observation direction. In particular, the generation of a micro-Doppler frequency comb by a hybrid magnetoelectric particle (HMEP) consisting of an SRR and a thin wire is studied. The HMEP, when illuminated by a plane wave from opposite directions, produces asymmetric backscattering [10], giving rise to completely different micro-Doppler combs detected in forward and backward directions (Fig. 1).

II. THEORETICAL FORMULATION

In this case, it can be shown that the field scattered by an object rotating about its center (position of the effective point dipole) has only one additional harmonic at $\pm 2\Omega$ (Ω is the angular rotation frequency) and it does not depend on the position of the detector (see, e.g., [8,11]). Objects with nontrivial internal structure can generate an entire frequency comb of micro-Doppler shifts with relative amplitudes

*pginzburg@post.tau.ac.il

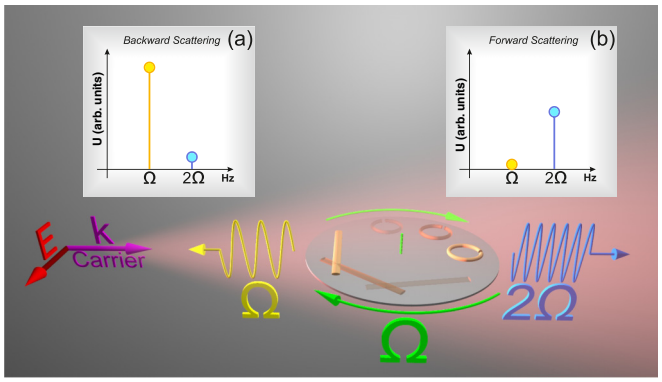

FIG. 1. Illustration of the generation of an asymmetric micro-Doppler comb by an axially rotating magnetoelectric particle (HMEP). The SRR and the wire constituting the HMEP are rotated with an angular frequency Ω in the polarization plane of the incident wave. The forward and backward scattered fields demonstrate different micro-Doppler spectra (insets show frequencies at the baseband).

dependent on the detection direction. To demonstrate this effect, a scatterer whose electromagnetic analysis requires at least two leading (and non-overlapping) dipole terms in the multipolar decomposition will be considered. While two dissimilar electric dipoles (EDs), separated by a wavelength-comparable distance could possess asymmetric back scattering, being illuminated from opposite sides, combination of electric and magnetic dipoles (MDs) was recently shown to provide an ultimate degree of asymmetry [10]. The HMEP under consideration consists of an SRR and a thin wire (Fig. 1). The electromagnetic response of the first one can be approximated by a MD, whereas the second constitutive element acts as an ED. The asymmetric reflection of the HMEP stems from the retarded coupling mechanism between ED and MD. It depends on the illumination wave frequency, the interparticle distance, and the individual parameters of the ED and MD. As a result, the backward scattering strongly depends on the particle orientation with respect to the incident wave **k** vector. Consequently, the signal has the periodicity of 2π (full angle of rotation) if Ω is normalized to unity. On the other hand, by virtue of the Lorentz reciprocity principle applied to particles that obey time-reversal symmetry, the field scattered in the forward direction has π periodicity. Therefore, θ and $\theta + \pi$ angles (HMEP major axis with respect to the **k** vector) provide the same forward scattered signal. As a result, the micro-Doppler comb will have completely different amplitudes of the peaks in the forward and backward directions. It is worth noting in brief that a similar behavior is expected from other types of particles. For example, the so-called Huygen's elements, relying on the interference between electric and magnetic dipolar responses that suppress the backward scattering [12,13], are expected to show a similar behavior if they do not possess circular symmetry (around rotational axis). Hence, it applies also to other metaparticles possessing nonsymmetrical scattering properties (e.g., Ω, Tellegen-Ω, and chiral-moving structures), which are discussed in detail in Refs. [14–16]. It is worth emphasizing, however, that in these additional examples, the electromagnetic description of a particle at rest still requires considering both EDs and MDs.

A. Adiabatic theory

To analyze the micro-Doppler comb generated by an HMEP in the forward and backward directions, an adiabatic approximation will be employed. Here, the set of static configurations will be analyzed, and the results will be stitched together, providing a 2π periodic function. This function (for either forward or backward scattering) will be decomposed into Fourier series, where the basic (lowest) discrete frequency corresponds to the angular velocity of the rotation.

A detailed analytical formulation of the scattering from two discrete dipoles constituting a HMEP is given elsewhere [10]. In the case of 0 or π orientation of the particle with respect to the incident wave direction, the scattered fields have simple analytical expressions. However, the case of an arbitrary angle is described by cumbersome expressions, which results from inversions of relevant matrices. In terms of the point dipole description applied to the geometry under consideration, the polarizabilities of the particles are given by

$$\overleftrightarrow{\alpha}_e = \alpha_{\mathrm{Wire}} \begin{pmatrix} \cos^2(\theta) & \frac{\sin(2\theta)}{2} & 0 \\ \frac{\sin(2\theta)}{2} & \sin^2(\theta) & 0 \\ 0 & 0 & 0 \end{pmatrix};$$
$$\overleftrightarrow{\alpha}_m = \alpha_{\mathrm{SRR}} \begin{pmatrix} 0 & 0 & 0 \\ 0 & 0 & 0 \\ 0 & 0 & 1 \end{pmatrix}, \quad (1)$$

where $\overleftrightarrow{\alpha}_e$ and $\overleftrightarrow{\alpha}_m$ are the polarizability tensors of the ED and MD, respectively; α_{Wire} and α_{SRR} are the intrinsic coefficients of the wire and SRR at rest (solely defined by their geometry at rest), and θ is the tilt angle of the HMEP with respect to the incident wave **k** vector. The structure lays in the XY plane, and the rotation vector is parallel to Z [Fig. 2(c)]. The MD tensor is assumed to be independent on the rotation angle, which is a reasonable approximation even for a single-slit SRR [17] [further symmetrization could be done using a double-slit geometry (see, e.g., [18])]. On the other hand, the ED tensor has two components, as the projection of the electric field on the wire does depend on the orientation. In principle, a HMEP consisting of a nonoverlapping pair of isotropic ED and MD will show a micro-Doppler behavior similar to the one discussed hereafter. The adiabatic theory is based on the matrix formulation [10] and the polarizability tensors taken from Eq. (1). The results are summarized in Fig. 2. The dimensions of the actual elements are the following: (i) the ring radius R_{SRR} is 9.5 mm, the slit width is 1 mm (ii), the wire length L_{Wire} is 60 mm, and they are used everywhere in what follows. All the elements were modeled as printed board elements on FR4 substrates. The polarizabilities α_{Wire} and α_{SRR} estimated from these parameters are shown in Figs. 3(a) and 3(b). Figure 2 summarizes typical results for the HMEP with the separation distance d between the wire and the ring equal to 38 mm. The structure is illuminated with 1.96 GHz carrier wave frequency. These parameters correspond to the maximal static asymmetry factor, as will be discussed below. Figures 2(a) and 2(b) shows the micro-Doppler comb for the given particle. The first odd peak at Ω is the most pronounced one in the backward scattered field [panel (a)], but it completely vanishes in the forward comb [panel (b)]. This behavior is quite fundamental and follows from the Lorenz reciprocity theorem, which predicts

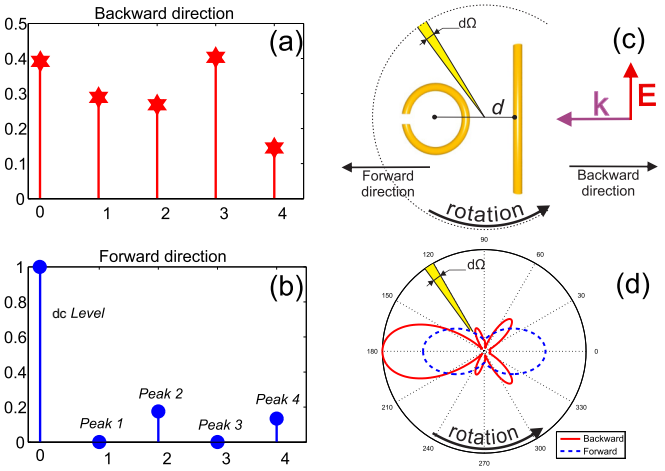

FIG. 2. Frequencies generation by an axially rotating magneto-electric particle (HMEP; analytic theory). Micro-Doppler frequency comb for the (a) backward and (b) forward scattering directions. Particle parameters: $d = 38\,\text{mm}, R_{\text{SRR}} = 9.5\,\text{mm}$, and $L_{\text{Wire}} = 60\,\text{mm}$; the illumination frequency is 1.96 GHz. (c) Schematic of the HMEP particle and the illumination field layout. (d) Polar plots of the absolute values of the scattered far field amplitudes versus the particle orientation with respect to the incident wave **k** vector. The red solid line and the blue dashed line correspond to the backward and the forward directions, respectively.

the signal to be an even function in Ω (θ and $\theta + \pi$ tilt angles of the particle with respect to the **k** vector lead to the same scattering). Consequently, all even peaks in the forward comb vanish, as it can be seen from Fig. 2(b). The Ω and 2Ω peaks in the backward comb are of most importance in this consideration [see Fig. 2(a)]. This behavior can be readily understood by looking at the polar plots [see Fig. 2(d)] that show the absolute values of the far-field amplitude in both the forward and backward directions (the angle corresponds to the orientation of the particle symmetry axis with respect to the **k** vector of the incident wave). Whereas the forward scattering diagram possesses a complete symmetry (with respect to the vertical axis), the backward case is completely asymmetric, showing the absolute values of the scattering amplitudes in the range from a maximum to an almost complete zero. The side lobes (in general, deviations from the cosine profile) are responsible for the occurrence of higher order peaks seen in panels (a) and (b).

Figure 2 shows the characteristic behavior of the micro-Doppler comb for one particular realization. In order to investigate the impact of the particle geometry on the comb, the scattering properties of the HMEP in the static regime should be invoked (this analysis follows the approach reported in Ref. [10]). First, the polarizabilities of the constitutive elements are estimated [see Figs. 3(a) and 3(b)] and used as parameters in the subsequent investigations. As previously discussed, the difference in backscattered field between the particle orientations at angles 0 and π is responsible for the occurrence of odd peaks. The static asymmetry factor (visibility) summarizing this behavior is defined as

$$V_a = \frac{\left|E_{\text{sc}}^B(\theta = 0)\right|^2 - \left|E_{\text{sc}}^B(\theta = \pi)\right|^2}{\left|E_{\text{sc}}^B(\theta = 0)\right|^2 + \left|E_{\text{sc}}^B(\theta = \pi)\right|^2}, \tag{2}$$

where E_{sc}^B are the far fields of the backscattered signals obtained for the opposite orientations of the HMEP. The color plot of V_a as a function of the separation distance between the elements and of the illumination frequency is given in Fig. 3(c). It can be clearly seen that the static asymmetry factor shows a pronounced resonance structure corresponding to both the resonances of the constitutive elements and the separation distance between them. For example, the parameters used for

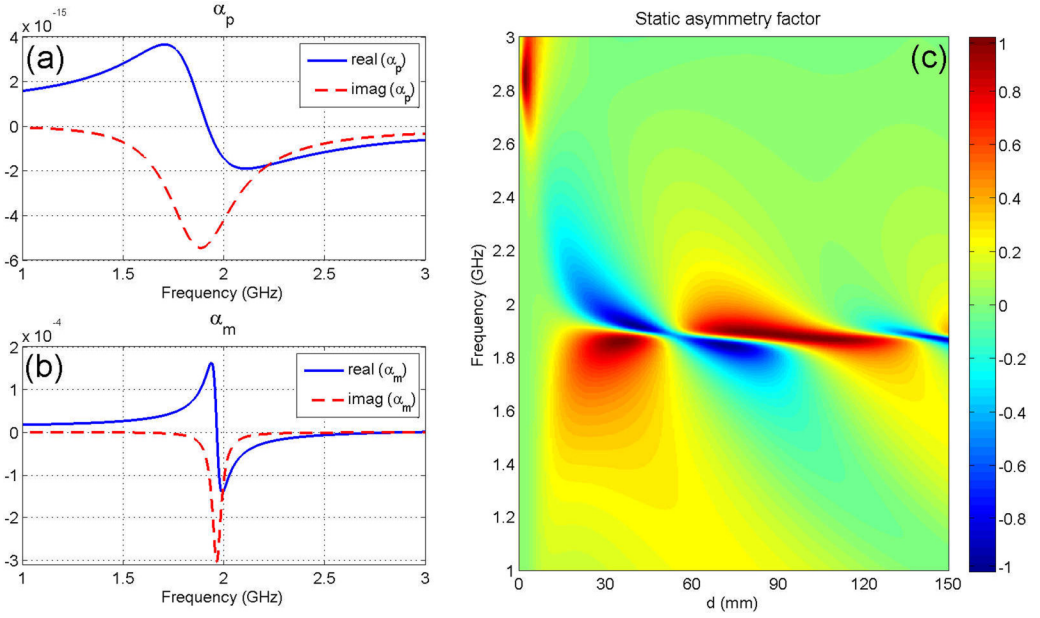

FIG. 3. Properties of the static configuration: (a) polarizability of the wire as a function of frequency, (b) polarizability of the split ring versus frequency, and (c) color map of the static asymmetry factor as a function of frequency (vertical axis) and separation distance between the wire and the ring (horizontal axis).

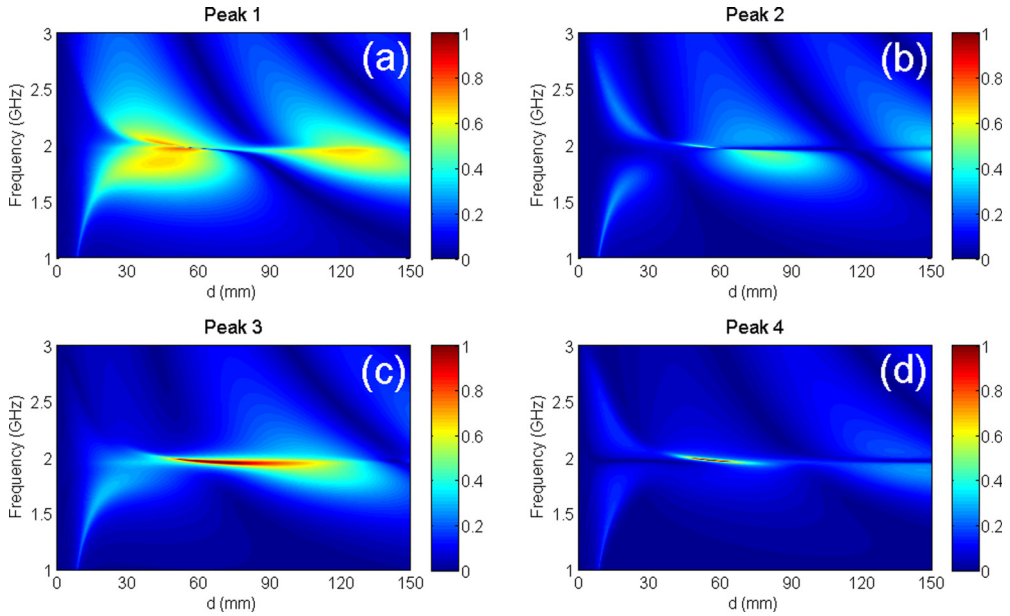

FIG. 4. Amplitudes of the micro-Doppler peaks in the backscattered signal from a HMEP as functions of the illumination frequency (vertical axis) and separation distance between the constitutive elements (horizontal axis): Color maps (a)–(d) refer, respectively, to the first, second, third, and fourth peak in the comb. All the amplitudes are normalized to the same value.

obtaining the results presented in Fig. 2 correspond to one of the maxima of the static asymmetry factor (bounded by definition [see Eq. (2)] between -1 and 1).

The adiabatic approach for deriving micro-Doppler combs enables investigating the properties of the peaks in relation to the parameters of the system. The first four peaks of the comb in the backscattered signal are shown in Fig. 4. The color maps present the peak amplitudes, normalized to the same value, as functions of the parameters used for plotting the map in Fig. 3. Figure 2(a) provides one point on each color map of Fig. 4. It can be seen that the micro-Doppler peaks are stronger in the regions where the HMEP possesses strong static asymmetry. This is an expected behavior, as the structure with this set of parameters scatters stronger. The first peak is much broader in the parametric space than the other three, as it encapsulates the major impact of the imbalance between the HMEP orientations at angles 0 and π.

The higher order peaks are related to the fast-oscillating features in the polar scattering diagrams [see, e.g., Fig. 2(d)], and consequently, they are more influenced by resonant effects. As a result, the higher-order peaks in the comb [see Figs. 4(b)–4(d)] are narrower. In addition, the higher-order peaks are sensitive to retardation effects (recall that a point dipole has a single second-order peak). It can be seen that the amplitudes of the higher-order peaks (e.g., of the third and fourth ones) are more pronounced at larger separation distance (d) between the HMEP constitutive elements.

B. Numerical modeling

The compact analytical model enables investigating the influence of a wide range of geometrical parameters on the micro-Doppler comb. However, it does not take into account the effects of substrates. The presence of additional layers with complex dielectric constants affects both the polarizabilities of the HMEP constitutive elements and the coupling between them. Several semianalytical models that consider these effects are available [10]. However, a full wave numerical simulation enables taking into account all the relevant effects (including finite sizes of constitutive elements) at the expense of computational time. A numerical model based on the finite element method follows exactly the same approach as the analytical one: scattered complex amplitudes, as the function of the static particle at an angle to the incident wave direction, are calculated and then Fourier transformed. After performing a set of straightforward numerical optimizations (not shown here), the particle dimensions were chosen to be $d = 38$ mm, $R_{\mathrm{SRR}} = 9.5$ mm, and $L_{\mathrm{Wire}} = 60$ mm (the same values were chosen in the theory). The material parameters for the thin copper strips and RF4 substrate were taken from widely available sources.

Figure 5 summarizes the results obtained for three different carrier frequencies: (i) 1.96 GHz, at which the particle has maximal backward-forward scattering asymmetry, (ii) 1.6 GHz, and (iii) 2.6 GHz, at which the particle is off resonance and the forward-backward difference in the micro-Doppler comb is expected to vanish. The insets in the panels of Fig. 5 show the angular dependent plots that were taken as the basis for the Fourier transform; the peaks at normalized frequencies are shown in the panels. It can be seen from the plots that the odd peaks are present only in the backscattered signal and only when the HMEP is in resonance with the illuminating wave. All other cases show signatures of even harmonics only, whereas the odd harmonic signatures either are on the numerical noise level (for the forward direction) or are small compared to the main contributions. A similar behavior was predicted by the analytical model. This very high sensitivity of the odd peaks to the resonant properties of the structure could serve as an additional channel for its remote probing.

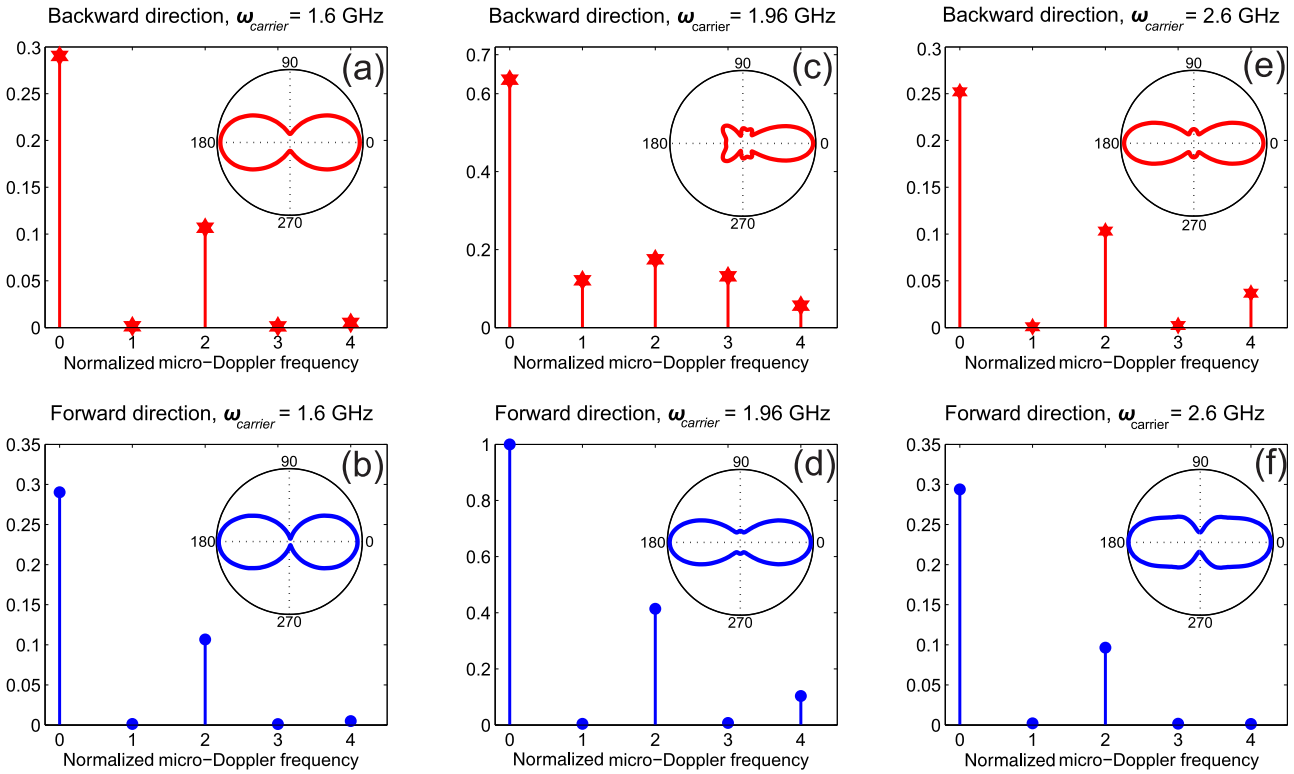

FIG. 5. Numerical modeling of micro-Doppler combs from a rotating HMEP particle on FR4 substrate: the amplitudes of the Fourier peaks at normalized frequencies. The upper row [panels (a), (c), and (e)] correspond to the backward direction, and the lower row [panels (b), (d), and (f)] to the forward direction. The columns correspond to different carrier frequencies: (a) and (b) 1.6 GHz, (c) and (d) 1.96 GHz (at which the particle has maximal backward-forward static scattering asymmetry), and (e) and (f) 2.6 GHz. The insets in the panels are angular-dependent scattering patterns (the polar angle is between the symmetry axis of the HMEP and the **k** vector of the incident wave).

III. EXPERIMENTAL RESULTS

Micro-Doppler combs in backward and forward directions were studied experimentally. The experiment was conducted in an anechoic chamber where an HMEP was positioned in the far fields of receiving and transmitting antennas. The HMEP was fabricated by chemical etching of a thin copper layer deposited on FR4 substrate [standard printed board circuit design; a photograph of the sample is given in the inset of Fig. 6(a)]. The HMEP was mounted on a motor shaft stabilized with a three-dimensional (3D)-printed plastic rack. The motor was controlled by a dc current, enabling rotational speeds of up to hundreds of Hertz. A constant angular frequency $\Omega = 2\pi \times 14\,\mathrm{Hz}$ was chosen for the experiment. The whole structure was placed between two horn antennas separated by a 2 m distance, ensuring that both the transmitting and the receiving horn were in the far field region of the scatterer. A vector network analyzer (VNA; Agilent E8362B) was used as a source of a 1.96 GHz continuous wave, feeding the transmitting antenna with the polarization set in the y direction. The output of the receiver (either a horn antenna in front or the same antenna for collecting the backward scattered field) was amplified and down-converted to the baseband by mixing it with the same 1.96 GHz carrier as in the incident field. The output of the mixer was passed through a low-pass filter to remove residual high frequencies and directed to a lock-in amplifier where the low-frequency spectral shifts of the scattered field were recorded. The backscattered signal was extracted from the measured complex-valued signals, obtained in several steps in order to eliminate instrumental responses. The calibration was performed with a large area metallic mirror, having a reflection coefficient equal to -1. All the reflected signals were normalized accordingly to factorize the impact of the measurement apparatus. In the case of dynamical experiments, the residual micro-Doppler shifts of the motor without the sample were subtracted from the data in order to factor out the influences of mechanical parts.

Figure 6 summarizes the experimental results. Panels (a) and (b) show micro-Doppler combs for backward and forward directions. It can be seen that the predominant peak in the forward case is indeed even, whereas the entire comb is observed in the backward direction, just as predicted theoretically. The residual odd peaks in panel (b) originate from mechanical instabilities, such as small drifts in the rotation speed and precession of the motor shaft. Panels (c) and (d) show experimental results for a simple rotating thin wire (a photograph is given in the inset) mounted on the same system. This investigation serves as a calibration test. A symmetrical structure, such as a wire, is not expected to demonstrate odd harmonics in either forward or backward directions. The experimental data confirm this prediction. It is worth noting that backscattering experiments are very sensitive to noise. The signals collected in the forward direction have much better signal-to-noise ratios. Furthermore, micro-Doppler harmonics are sensitive to even a slight displacement of the object violating the symmetry. The higher-order peaks are also influenced by the drifting angular velocity of the

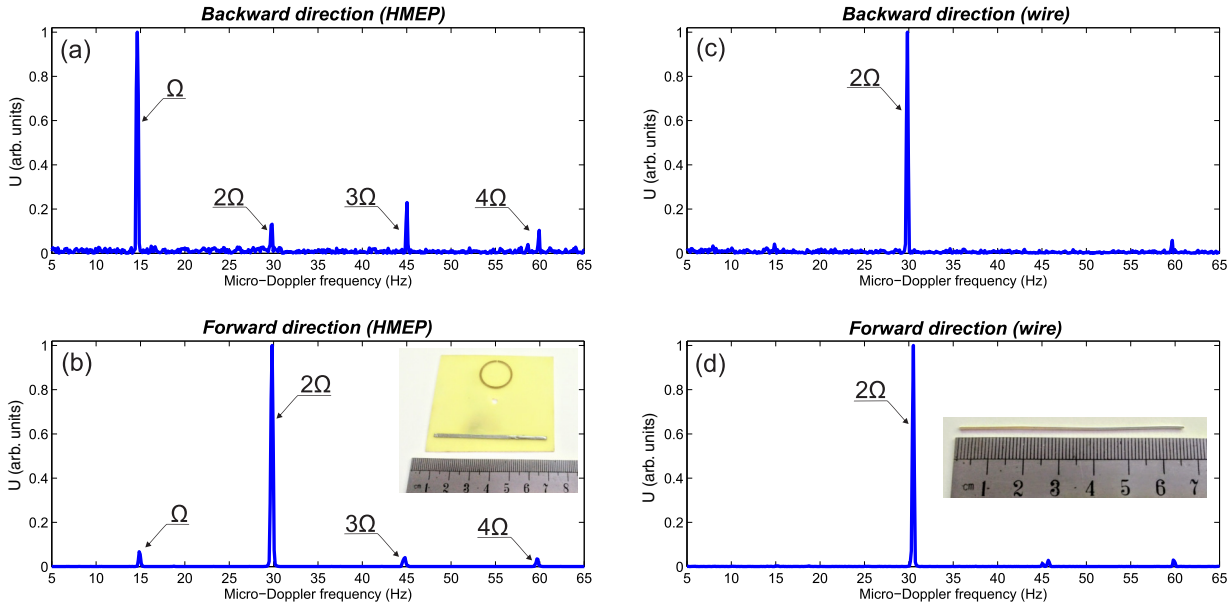

FIG. 6. Experimental observation of the micro-Doppler combs. (a) and (b) The HMEP particle, (c) and (d) the thin metal wire. Upper row is the backward direction, lower row is the forward direction. The angular frequency of mechanical rotation is $\Omega = 2\pi \times 14$ Hz. The insets show photographs of the samples.

motor (instabilities) and by parasitic precessions of the motor shaft. All these parameters affect the micro-Doppler combs, especially in resonant systems that amplify noise.

IV. OUTLOOK AND CONCLUSIONS

Electromagnetic scattering from axially rotating magneto-electric particles was studied analytically, numerically, and experimentally. It was shown that a rotational (accelerated) motion gives rise to micro-Doppler frequency comb generation. The properties of the combs were studied by considering two detection directions (bistatic configuration). In particular, the forward (a collecting antenna is in front of the source) and backward (signal collection and illumination are performed with the same antenna) cases were investigated. It was shown that the signal collection in the backward direction provides more information about the scatterer. In particular, the collection of odd micro-Doppler harmonics in the forward case can be missed by virtue of the Lorenz reciprocity principle, whereas the backward detection is free of these limitations. Collecting data from several observation points enlarges the amount of information that can be used for further investigations. In addition, resonant properties and retardation effects were shown to have signatures in higher-order micro-Doppler harmonics.

Characterization of rotating electromagnetic scatterers by means of micro-Doppler spectra in bistatic and multistatic configurations (several detection directions) could serve as a powerful tool in remote sensing and spectroscopy. Careful analysis utilizing the mechanical motion of detected objects enables extracting extended information on their internal structure, similar to approaches used in synthetic aperture radars (SARs).

ACKNOWLEDGMENTS

This paper was supported in part by TAU (Rector Grant), the PAZY Foundation, the KAMIN Project, and the German-Israeli Foundation (GIF; Grant No. 2399). The numerical calculations were supported in part by the Russian Foundation for Basic Research (Project No. 16-52-00112). The calculations of magnetic field distributions and multipole moments were supported by the Russian Science Foundation (Grant No. 16-12-10287).

[1] J. G. Van Bladel, *Electromagnetic Fields*, 2nd ed. (Wiley-IEEE Press, New Jersey, 2007).

[2] P. G. Bergmann, *Introduction to the Theory of Relativity* (Dover Publications, New York, 1976).

[3] M. A. Richards, *Fundamentals of Radar Signal Processing*, 2nd ed. (McGraw-Hill Education, New York, 2014).

[4] A. Stefanov and S. Member, IEEE Trans. Antennas Propag. **49**, 688 (2001).

[5] G. Greving, W. D. Biermann, and R. Mundt, in *Proceedings of the 2012 International Conference on Electromagnetics in Advanced Applications, Cape Town* (IEEE, New York, 2012), pp. 416–419.

[6] G. A. Somers and D. M. Bruno, in *Proceedings of the IEEE Antennas and Propagation Society International Symposium and URSI National Radio Science Meeting, Seattle, WA* (IEEE, New York, 1994), Vol. 1, pp. 144–147.

[7] V. C. Chen, F. Li, S. S. Ho, and H. Wechsler, in *Proceedings of the IEEE Transactions on Aerospace and Electronic Systems* (IEEE, New York, 2006), Vol. 42, pp. 2–21.

[8] V. Kozlov, D. Filonov, Y. Yankelevich, and P. Ginzburg, J. Quant. Spectrosc. Radiat. Transf. **190**, 7 (2017).

[9] A. P. Slobozhanyuk, P. V. Kapitanova, D. S. Filonov, D. A. Powell, I. V. Shadrivov, M. Lapine, P. A. Belov, R. C. McPhedran, and Y. S. Kivshar, Appl. Phys. Lett. **104**, 014104 (2014).

[10] V. Kozlov, D. Filonov, A. S. Shalin, B. Z. Steinberg, and P. Ginzburg, Appl. Phys. Lett. **109**, 203503 (2016).

[11] R. G. Newburgh and G. V. Borgiotti, *Physical Sciences Research Papers Air Force Cambridge Research Labs.* (Hanscom AFB, MA, 1975).

[12] A. E. Krasnok, A. E. Miroshnichenko, P. A. Belov, and Y. S. Kivshar, Proc. SPIE **8806**, 880626 (2013).

[13] A. O. Karilainen, P. Alitalo, and S. A. Tretyakov, in *Proceedings of the 5th European Conference on Antennas and Propagation (EUCAP), Rome* (IEEE, New York, 2011), pp. 1865–1868.

[14] Y. Ra'di, S. Member, V. S. Asadchy, and S. A. Tretyakov, IEEE Trans. Antennas Propag. **61**, 4606 (2013).

[15] Y. Ra'di, S. Member, V. S. Asadchy, and S. A. Tretyakov, IEEE Trans. Antennas Propag. **62**, 3749 (2014).

[16] Y. Ra'di, V. S. Asadchy, and S. A. Tretyakov, Phys. Rev. B **89**, 075109 (2014).

[17] K. Aydin, I. Bulu, K. Guven, M. Kafesaki, C. M. Soukoulis, and E. Ozbay, New J. Phys. **7**, 168 (2005).

[18] B. Sauviac, C. R. Simovski, and S. A. Tretyakov, Electromagnetics **24**, 317 (2004).